The Susceptibility of Copper to Pitting Corrosion in Borate-Buffered Aqueous Solutions Containing Chloride and Sulfide

M. Guo,[1,*] J. Chen,[1] T. Martino,[1,a] M. Biesinger,[2] J. J. Noël,[1,2,,z] and D. W. Shoesmith[1,2,***]**

[1] *Department of Chemistry, The University of Western Ontario, London, Canada*
[2] *Surface Science Western, The University of Western Ontario, London, Canada*

The formation of sulfide and oxide films on copper (Cu) was studied in chloride solutions with and without added borate and sulfide. Electrochemical experiments demonstrated that Cu sulfide (Cu_2S) films formed at considerably lower potentials than oxides (Cu_2O/CuO) films. The growth of Cu_2S was controlled by a combination of sulfide transport to the reacting Cu surface and the competition between SH^- and Cl^- ions for adsorption sites on the Cu surface. Scanning electron microscopy on focused ion-beam cut cross sections demonstrated that the films were porous and not passive. At more positive potentials, Raman spectroscopy and X-ray photoelectron spectroscopy demonstrated that the formation of oxide films, likely with the formation of a passive oxide film, dominated over anodic dissolution of Cu as Cu^I chloride complexes when the borate to chloride concentration ratio was sufficiently high. If pitting is to occur on Cu, it will require oxide not sulfide film growth.
 [DOI: 10.1149/2.0611915jes]

Manuscript submitted May 28, 2019; revised manuscript received October 24, 2019. Published November 6, 2019.

The safe management and disposal of high-level nuclear waste is essential if nuclear power is to remain a viable energy source. The proposed method in many countries, including Sweden, Finland and Canada, is to bury the spent nuclear fuel discharged from reactors in a deep geologic repository (DGR) with multiple barriers to provide safe isolation and containment. A primary barrier in this sequence is a corrosion-resistant waste container able to withstand the anticipated hydrostatic, lithostatic and glacial loads. In the Swedish KBS-3 concept, the spent fuel will be sealed in a container comprising a cylindrical Cu shell (50 mm in thickness) and a load-bearing inset of nodular cast iron.[1]

Immediately after emplacement, the container, which contains the heat-generating fuel, will be exposed to humid aerated conditions which will rapidly evolve to cool and anoxic as radiation fuels decay and heat production decreases.[2] Once the O_2 trapped upon emplacement has been consumed by microbial and mineral reactions within the clay surrounding the container and by minor container corrosion,[2] the long-term threat to the durability of the container will be SH^-. The Swedish and Finnish DGRs are known to contain SH^-, produced in the groundwater as a consequence of sulfate-reducing bacteria and, possibly, mineral dissolution processes.[3] The SH^- concentration, $[SH^-]$, is conservatively estimated to be $\leq 10^{-5}$ M based on measurements in groundwaters from the proposed Swedish Forsmark site[4] with $[Cl^-]$ in the range of 0.1 to 0.3 M.[3,5]

Corrosion of Cu in aqueous SH^- solution is driven by the formation of chalcocite (Cu_2S) films with their structure and properties being determined by the rate of SH^- transport to the Cu surface relative to its interfacial reaction rate with Cu, and the competition for surface adsorption sites between SH^- and Cl^-, and possibly other anions.[6] Films grown electrochemically exhibit similar dependencies on $[SH^-]$, $[Cl^-]$ and the transport of SH^-,[7,8] with passive films possible only at high $[SH^-]$ ($\geq 5 \times 10^{-4}$ M) and transport fluxes, conditions unachievable in a DGR with a bentonite buffer in place. More recent studies indicate that, even at these high $[SH^-]$, the Cu_2S films formed are porous rather than passive.[8]

This conclusion is at odds with views expressed by other researchers who claim that passive sulfide films do form leading to Cl^- induced film breakdown and a susceptibility to pitting. They also claimed this susceptibility increased with $[Cl^-]$ and temperature.[9–12] In some of these studies,[9,10] the solution pH was buffered with borate which may have significantly altered the film growth process. The corrosion/electrochemical behavior of Cu is known to be modified by the adsorption of anions and pitting has been demonstrated to be possible on Cu in borate-buffered solutions.[13–15] In addition, Qin et al.[16] demonstrated that an increase in alkalinity could increase the probability of passivation of Cu but in the absence of SH^-.

The primary goal of this study is to determine whether passive Cu sulfide films can be formed when Cu is electrochemically polarized in aqueous SH^- solutions containing Cl^- and whether they then undergo Cl^- induced passive film breakdown. To facilitate comparison to the published literature, solutions used in this work are identical to those used in previous studies where it is claimed such processes occurred.[9,10]

Experimental

Sample preparation.—Cu used in all experiments is O-free and P-doped (30-100 wt.ppm) and provided by the Swedish Nuclear Fuel and Waste Management Co (SKB), Solna, Sweden. Cu electrodes for rotating disk electrode (RDE) experiments were machined as disks, with a threaded connection to a Ti rod and sealed into a Teflon holder using epoxy resin. A nonconductive lacquer was applied to prevent exposure of the steel/Cu junction to the electrolyte, leaving a flat Cu surface with a total surface area of 0.785 cm^2 exposed to the electrolyte. Prior to an experiment, the Cu electrode was ground with a sequence of SiC papers with grit sizes 800, 1000, 1200, 2400, 4000, and then polished to a mirror finish using aluminum oxide (Al_2O_3) suspensions with decreasing particle sizes (1 μm, 0.3 μm, and 0.05 μm), rinsed with Type I water with a resistivity of 18.2 MΩ·cm (provided by a Thermo Scientific Barnstead Nanopure 7143 ultrapure water system), sonicated with methanol for 1 min and finally dried in a stream of ultrapure Ar gas.

Electrochemical cell, instrumentation, and procedures.—Experiments were performed in a standard three-electrode cell using a Cu RDE as working electrode, a Pt plate as counter electrode, and a saturated calomel reference electrode (SCE, 0.242 V vs SHE (Standard

*Electrochemical Society Student Member.
**Electrochemical Society Member.
***Electrochemical Society Fellow.
[a]Present address: CanmetMATERIALS, Natural Resources Canada, Hamilton, ON l8P 0A5, Canada.
[z]E-mail: jjnoel@uwo.ca

Hydrogen Electrode)). Electrochemical experiments were performed inside a Faraday cage to reduce interference from external electrical noise. The RDE rotation rate (ω) was controlled by a Pine Instrument Company Analytical Rotator Model AFA86 Serial 882. Cyclic voltammetric (CV) experiments were conducted using either a Solartron 1287 potentiostat or a Solartron Analytical Modulab equipped with CorWare and XM-Studio-ECS software. Prior to experiments, the Cu electrode was cathodically cleaned at −1.5 V vs SCE for 1 min to reduce air-formed oxides, and then at −1.15 V vs SCE for another minute to allow the detachment of any H_2 bubble which may have formed due to H_2O reduction at the more negative potential. CVs were performed from an initial potential of −1.35 V vs SCE to various anodic limits at a scan rate of 2 mV/s. All experiments were conducted at room temperature (21 ± 2°C).

Solutions.—Solutions were prepared with reagent-grade sodium chloride (NaCl, 99.0% assay), sodium sulfide ($Na_2S{\cdot}9H_2O$, 98.0% assay), boric acid (H_3BO_3, 99.5% assay), sodium borate decahydrate ($Na_2B_4O_7{\cdot}10H_2O$, 99.5% assay) and Type I water (18.2 MΩ·cm). Electrodes were exposed to 2×10^{-4} M SH^- solutions (pH = 9) containing various chloride concentrations in the range from 0.01 M to 5 M. To ensure the maintenance of an anoxic environment, and to minimize SH^- oxidation, solutions were purged with ultra high purity (99.999%) Ar for 30 min prior to each experiment and then continuously throughout the experiments.

Surface analysis.—Scanning electron microscopy (SEM) analyses were performed using a Leo 1540 instrument equipped with a focused ion beam (FIB) (Zeiss Nano Technology Systems Division, Germany) at the Western Nanofabrication Facility. An electron beam with an accelerating voltage ranging between 1 kV and 5 kV was used to collect high-resolution images of both film morphologies and milled samples. Chemical compositions of sample surfaces were qualitatively analyzed by energy dispersive X-ray spectroscopy (EDX) using a Leo 1540 FIB/SEM microscope.

Raman spectroscopy was performed using a Renishaw 2000 Raman spectrometer equipped with a 633 nm He-Ne laser and an Olympus microscope. Spectra were obtained using a 50 × uncoated objective lens with the beam focused to a diameter of ~2 μm. To minimize any surface heating effects, the laser was used at 10% power. Prior to the acquisition of spectra, the spectrometer was calibrated against the 520.5 cm^{-1} peak of Si.

X-ray photoelectron spectroscopic (XPS) analyses were performed with a Kratos AXIS Nova spectrometer using an Al K_α monochromatic high energy (hν = 1486.6 eV) source (15 mA, 14 kV). The instrument work function was calibrated using the Au $4f_{7/2}$ line (Binding Energy (BE) = 93.95 eV) and the spectrometer dispersion was adjusted using the Cu $2p_{3/2}$ peak with BE = 932.63 eV. The C 1s peak at 284.8 eV was used as a standard to correct for surface charging. High resolution spectra were obtained for the Cu 2p peaks at a pass energy of 160 eV. Spectra were analyzed using CasaXPS software as described elsewhere[17] with a standard Shirley background correction. Cu $L_3M_{4,5}M_{4,5}$ Auger spectra were also recorded and treated as described elsewhere.[17]

Results

Borate-buffered chloride solutions.—Figure 1 shows CVs recorded in slightly alkaline 0.1 M Cl^- solutions (pH = 9, adjusted by the addition of NaOH solution with and without added borate) at rotation rate ω = 33 Hz. In the absence of borate, the anodic current (*i*) in the potential (*E*) range −0.25 V vs SCE to −0.1 V vs SCE increased exponentially with *E* on the forward scan and retraced the *i*-*E* relationship on the reverse scan. This behavior was that expected for an active dissolution process. In the *E* range from −0.25 V vs SCE to −0.6 V vs SCE on the reverse scan, a shallow reduction process (C1) was observed suggesting the presence of surface intermediates formed during the anodic dissolution process. The active dissolution of Cu is known to involve adsorbed Cl^- species and to proceed via the

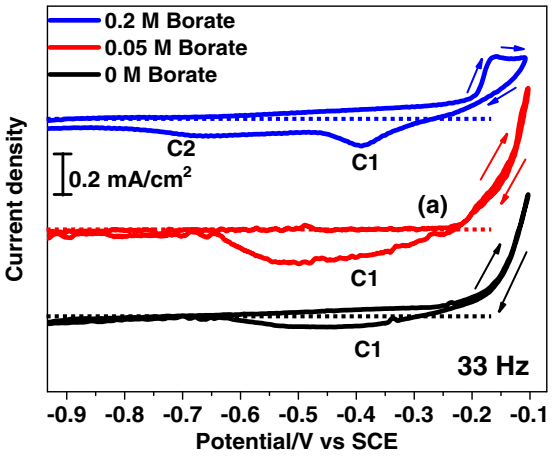

Figure 1. CVs performed in slightly alkaline (pH 9) 0.1 M chloride solutions containing various $[BO_3]_{tot}$.

formation of a thin surface CuCl layer,[18]

$$Cu + Cl^- (aq) \rightarrow CuCl\,(ads) + e^- \quad [1]$$

$$CuCl\,(ads) + (x\text{-}1)\,Cl^- (aq) \rightarrow CuCl_x{}^{(x-1)^-} (aq) \quad (x = 1,\ 2,\ \text{or}\ 3) \quad [2]$$

Surface $CuCl_{ads}$ species can be formed at potentials more negative than that predicted based on the thermodynamic properties of bulk CuCl. This mechanism has been shown to be valid over a wide range of chloride concentrations from 0.001 M to 5.0 M,[3] with x increasing as the chloride concentration increases. The breadth (on the potential scale) of the shallow reduction process suggested the presence of more than one surface species since, as the pH becomes more alkaline, hydrolysis of adsorbed $CuCl_{ads}$ species to $Cu(OH)_{ads}$ can occur as a precursor to Cu_2O formation,

$$CuCl\,(ads) + OH^- (aq) \rightarrow Cu\,(OH)\ (ads) + Cl^- (aq) \quad [3]$$

$$2Cu\,(OH)\,(ads) \rightarrow Cu_2O\,(s) + H_2O \quad [4]$$

When a small concentration of borate ($[BO_3]_{tot}$) was added, similar anodic behavior was observed but with a slightly enhanced current, especially at the *E* at which the current began to rise (indicated as (a) in Figure 1). The suggestion (above) that a mixture of surface intermediates could have been formed was supported by the enhancement of the surface coverage (indicated by the increase in charge associated with their reduction (C1) on the reverse scan). Since borate would not be expected to promote Cl^- adsorption, this suggested a displacement of adsorbed Cl^- by borate adsorption leading to enhanced coverage by Cu(OH)(ads), i.e., a preference for Reaction 3 rather than Reaction 2. When the $[BO_3]_{tot}$ was increased further to a value >[Cl^-], a partial passivation process was observed, leading to a more distinct C1 peak and a further reduction process (C2) at more negative potentials.

To confirm the presence of oxides, Raman spectroscopy was performed on a Cu electrode after a potential scan to −0.1 V vs SCE in borate-free 0.1 M Cl^- solutions (pH = 9) with the pH controlled by addition of NaOH, Figure 2. The presence of Cu_2O was demonstrated by the broad peak doublet in the range 490 cm^{-1} to 650 cm^{-1}, with the exact peak positions reported in the literature varying between studies, but very close to those in Figure 2 when measured using surface-enhanced Raman spectroscopy.[19,20] Since CuO can also exhibit a peak (generally weak) in this area, identification of CuO was confirmed by the peak at 297 cm^{-1}[21–23] which was not compromised in this manner. The presence of these oxides did not rule out the possibility that unhydrolyzed CuCl may also have been present on the oxidized surface. Once the dissolution of Cu^I (as $CuCl_x{}^{(x-1)-}$) was hindered, the

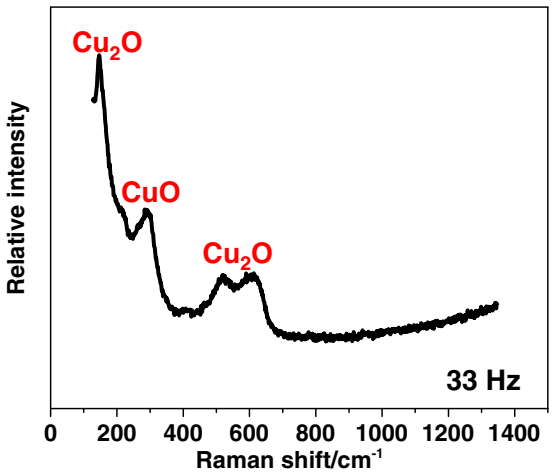

Figure 2. A Raman spectrum collected on a Cu sample after scanning the potential from −1.35 V vs SCE to −0.10 V vs SCE in a 0.1 M NaCl solution (pH = 9).

formation of Cu_2O/CuO was expected based on the *E*-pH diagram[24] and the extremely low solubilities of both oxides at pH = 9.[25,26]

Borate-buffered chloride solutions containing sulphide.—Figure 3 shows a CV recorded in a 0.1 M NaCl solution containing 0.2 M borate and 2×10^{-4} M SH^- (pH = 9) at rotation rate ω = 33 Hz. This solution composition was chosen to facilitate a comparison to a set of potentiodynamic polarization experiments conducted in a solution with the same composition by Mao et al.[9] Their experiments were conducted in nitrogen-sparged solutions and only the forward scan from −1.35 V vs SCE to −0.10 V vs SCE was recorded.

Six distinct regions of behavior were observed. Region 1 has been shown to be due to the anodic formation of a Cu_2S (chalcocite) surface layer[8,27] with the formation of oxides/hydroxides and soluble chloride complexes thermodynamically prohibited in this potential range.[24] As shown in Figure 4a, the anodic current in this region was independent of *E* but dependent on ω, confirming, as observed previously, but only for potentials up to −0.7 V vs SCE,[8] that the reaction was at least partially transport-controlled. It was also shown previously that,[8] if the CV scan was reversed in region 1, the current was maintained on the reverse scan, leading to further sulfide film growth. Such a feature would only have been possible if the Cu_2S film remained porous and non-passive, and was able to sustain film growth at the Cu_2S/solution

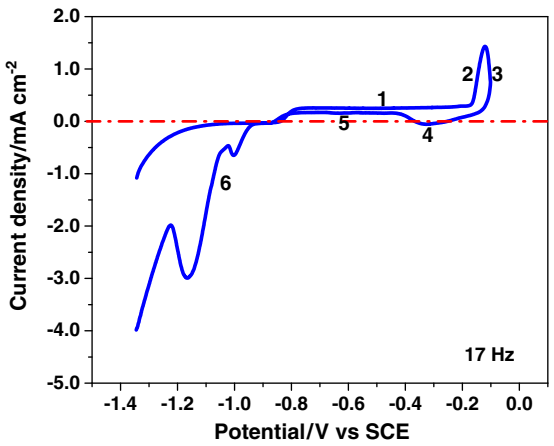

Figure 3. CVs performed in a solution containing 0.1 M NaCl + 2×10^{-4} M Na_2S + 0.2 M borate (pH 9) at 20°C, and at rotation rate ω = 17 Hz. Six distinct regions were observed.

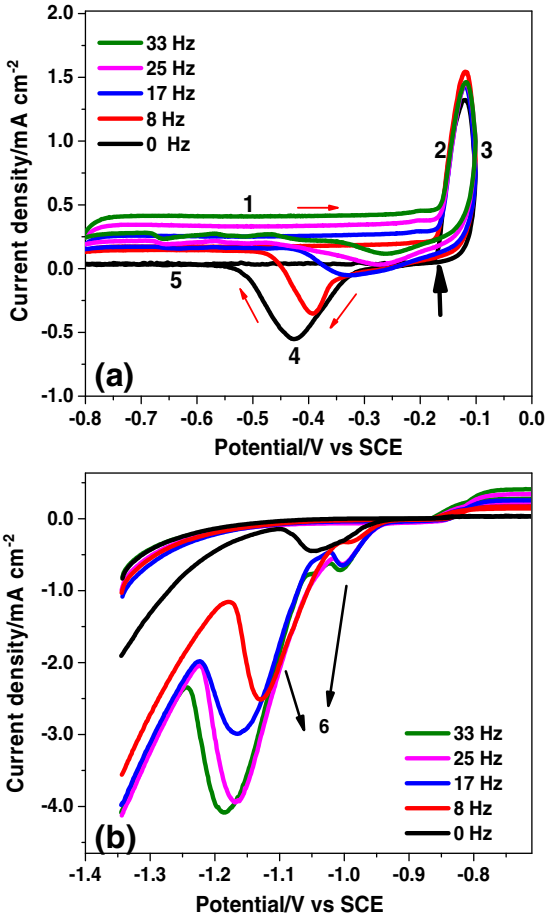

Figure 4. CVs performed in solutions containing 0.1 M NaCl + 2×10^{-4} M Na_2S + 0.2 M borate (pH 9) at 20°C at various values of ω.

interface.[8] If the film formed on the forward scan had been passive, the current on the reverse scan would have been effectively zero, since the electric field within such a film would have been too low to sustain the further film growth observed. Although not shown here, this reversibility was maintained up to the onset of region 2 confirming that passivity was not achieved throughout region 1. The crystalline nature of the Cu_2S film anodically-formed in this E[28] region was consistent with growth by deposition at the film/solution interface supported by the transport through solution of Cu^I, as both sulfide complexes ($Cu(SH)_2^-$) and Cu_3S_3 clusters, formed at the Cu surface.[29,30] Cu_3S_3 clusters have also been shown to be involved in the corrosion of Cu in aqueous sulfide solutions and their function as intermediates in Cu_2S formation have been demonstrated.[29,30] All these features confirm that the current in region 1 was not a passive current.

When *E* entered region 2, and $CuCl_x^{(x-1)-}$ and oxide film formation was possible, the current became independent of ω but steeply dependent on *E*, Figure 4a. The lack of a dependence on ω would be expected for reactions which occurred within the pores of the previously deposited Cu_2S film. Additionally, the *E* at which region 2 commenced was independent of ω demonstrating that the current increase was not influenced by the increased flux of species such as SH^- and Cl^- to the Cu surface. The decrease in current in region 3 indicated the occurrence of a similar partial passivation process to that observed in the absence of SH^- (Figure 1). The minor dependence of the current on ω in this region, especially on the forward scan, confirmed that this partial passivation process was considerably less dependent on the transport of SH^- to the electrode surface compared to the current for Cu_2S film growth in region 1. As demonstrated in the absence of SH^-, Figures 1 and 2, this partial passivation process could be attributed

to the formation of an oxide film. Given the limited [SH^-] at the Cu surface compared to [Cl^-] and [BO_3]$_{tot}$, it was likely that the direct formation of Cu_2S via the reaction steps functioning in region 1 was reduced somewhat in region 2.

The reduction peak in region 4 (Figure 4a) could be attributed to the cathodic reduction of anodically-formed $CuCl_x^{(x-1)-}$ trapped within the pores in the Cu_2S film and the reduction of the passivating oxide film formed on the Cu surface beneath the Cu_2S film. As opposed to the anodic process (regions 2 and 3), the reduction process (region 4) was strongly dependent on ω, the cathodic charge associated with the peak decreasing markedly as ω increased. Under stagnant conditions, when the formation of Cu_2S in regions 2 and 3 was limited due to transport control by SH^- to the Cu surface, the anodic charge consumed in regions 2 and 3 was approximately equal to the cathodic charge regained in region 4. This indicates that the species formed anodically was trapped within the pores of the Cu_2S film and available for reduction in region 4. Since a passive oxide would be expected to be thin, its formation would only have required a small amount of anodic charge. Consequently, the great majority of the anodic charge consumed in regions 2 and 3 could be attributed to the formation of soluble $CuCl_x^{(x-1)-}$, and of the cathodic charge consumed in region 4 to its reduction on the reverse scan.

When ω was increased, the cathodic charge associated with the reduction peak in region 4, Figure 4a decreased markedly and the overall current eventually became positive. This switch in sign could be attributed to a combination of features: (i) the loss of $CuCl_x^{(x-1)-}$ by transport to the bulk of solution, which would have limited its cathodic reduction on the reverse scan; and (ii) the enhanced transport of SH^- into the porous structure, which would have enhanced Cu_2S formation. This second process would also have led to the reaction

$$2CuCl_x^{(x-1)^-}\left(aq\right) + SH^-\left(aq\right) \rightarrow Cu_2S\left(s\right) + 2xCl^-\left(aq\right) + H^+\left(aq\right) \quad [5]$$

with the Cu_2S formed stable in region 4, and hence not reduced until potentials in region 6 were reached. Reaction 5 has been shown previously to be rapid.[29] In addition, any Cu_2O formed would be chemically transform to Cu_2S by the reaction:

$$Cu_2O\left(s\right) + SH^-\left(aq\right) \rightarrow Cu_2S\left(s\right) + OH^-\left(aq\right) \quad [6]$$

albeit at a much slower rate than that of Reaction 5, as previously shown.[31]

Once the species produced within the porous film was reduced in region 4, an anodic current for further Cu_2S film growth became observable in region 5, leading to an increase in the charge associated with the film reduction peak in region 6. This confirmed that the Cu_2S film formed on the forward scan, whose growth would have continued throughout regions 2, 3 and 4, remained porous. While not as large as on the forward scan, the current was dependent on ω, demonstrating that the film growth process remained partially transport-controlled on the reverse scan. This provided unequivocal evidence that current decrease in region 3 was not due to the formation of a passive Cu_2S film.

Finally, in potential region 6, two cathodic reduction peaks were observed, Figure 4b, for the reduction of the Cu_2S film. The charges associated with Cu_2S film reduction were considerably greater than observed in our previous study,[8] when the potential was reversed at −0.7 V vs SCE. This demonstrated that the formation of a porous Cu_2S layer continued when the potential limit was extended to −0.1 V vs SCE. In addition, the charge increased with electrode rotation rate, Figure 4b, as expected if anodic film growth occurred, at least partially, under transport control on both the forward and reverse scans. The origin of these two reductions peaks has been discussed previously.[8]

The influence of chloride on sulfide film formation.—Figure 5 shows a plot of the current recorded at $E = -0.7$ V vs SCE and rotation rate $\omega = 17$ Hz as a function of [Cl^-] in CVs similar to those shown in Figures 3 and 4. Similar behavior was observed at other values of ω in the range 8–33 Hz. Within the chloride concentration range investigated (0.1 M to 5.0 M), the current density was well below

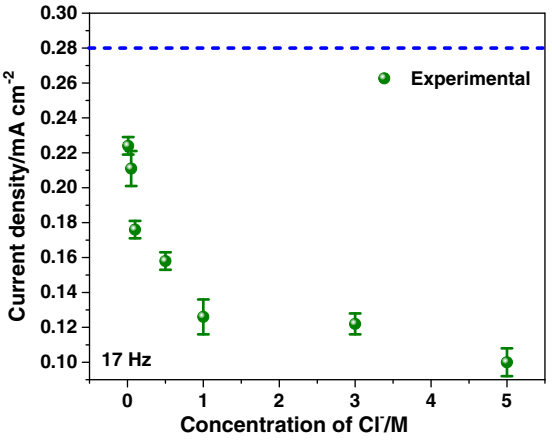

Figure 5. Limiting current densities at E = −0.7 V vs SCE (region 1, Figure 3) plotted as a function of [Cl^-] taken from CVs conducted in borate-buffered (pH 9) solutions containing 2×10^{-4} M SH^- but at various [Cl^-]. The dashed line shows the value for a total transport-controlled reaction calculated using the Levich equation.

the theoretical transport-controlled value (calculated using the Levich equation), dependent on the value of ω (as shown in Figure 4a) and decreased as chloride concentrations increased. This influence of [Cl^-] was the opposite of that observed by Kong et al.[32] who showed that the current increased with [Cl^-] when Cu was covered by an oxide film. Their increase in current was attributed to a chloride-induced increase in the cation vacancy density and the diffusion rate of Cu vacancies in the oxide, the clustering of which at the metal/oxide interface was considered necessary for passive film breakdown and the initiation of pitting. Such an explanation cannot account for our observations. These authors also showed a slight increase in current with [Cl^-] when a Cu_2S film was present, which is also at odds with the results in Figure 5. However, since their experiments were conducted under nitrogen-sparged conditions, the interfacial [SH^-] at the Cu surface would have been depleted at the base of pores in the thickening Cu_2S deposit and, consequently, not representative of the bulk solution [SH^-]. Since Cl^- was not consumed in this potential region, the [Cl^-] at the Cu surface would have been maintained, leading to a high [Cl^-]/[SH^-] ratio, a situation that would cause an enhanced porosity of the Cu_2S film.[5] We conclude that, in our case, the sulfide film growth process was partially controlled by SH^- transport to the reacting Cu surface and partially by competition for Cu surface adsorption sites between SH^- and Cl^- which impeded the initial charge transfer reaction

$$Cu\left(s\right) + SH^-\left(aq\right) \rightarrow Cu\left(SH\right)\left(ads\right) + e^- \quad [7]$$

in the overall film formation process. The ability of Cl^- to adsorb on Cu is well established.[22,33,34] This combination of features required that the Cu_2S film remained porous and able to support film growth by deposition at the Cu_2S/solution interface, as has been previously demonstrated.[7]

The influence of chloride on Cu^I dissolution and oxide film formation.—Figure 6 shows sections of CVs recorded at $\omega = 17$ Hz in a borate-buffered solution (0.2 M, pH = 9) containing 2×10^{-4} M SH^- and various [Cl^-]. The influence of Cl^-, while subtle in the region of Cu_2S growth (Figure 5), had a dramatic effect in regions 2 and 3 (defined in Figure 3). At low [Cl^-] (0.01 M, 0.05 M, 0.1 M), an active-to-passive transition was observed indicating the formation of a partially passive oxide as observed in the absence of SH^- at this [BO_3]$_{tot}$, Figure 1. Cathodic reduction of this oxide led to only a shallow current on the reverse potential scan as observed in the absence of SH^- (Figure 1). When the [Cl^-] was increased to 0.5 M and 1.0 M, a considerably larger anodic current was observed but the active-to-passive transition still occurred at 0.5 M. At 1.0 M, this transition was

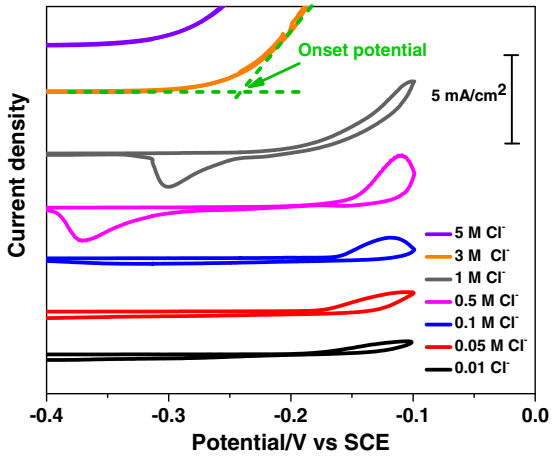

Figure 6. CVs conducted at rotation rate $\omega = 17$ Hz in 2×10^{-4} M SH^- + 0.2 M borate solution containing various [Cl^-]s.

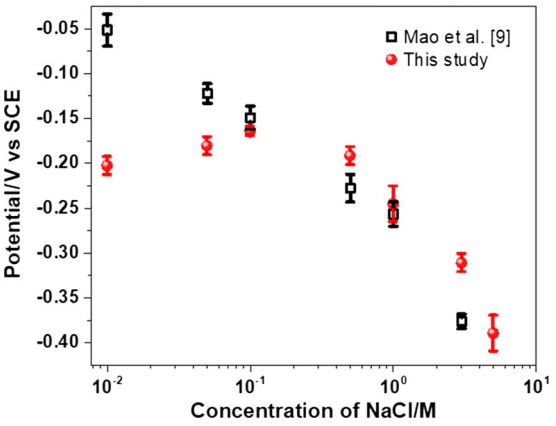

Figure 7. Comparison of the potentials at which the current increases in CVs (Figure 6) to those measured by others and claimed to be SH^- film breakdown potentials.

no longer observed. For both 0.5 M and 1.0 M, a significant reduction process was observed on the reverse scan consistent with the accumulation of $CuCl_x^{(x-1)-}$ in pores in the Cu_2S film on the forward scan (as discussed above) and its reduction on the reverse scan. At even higher [Cl^-] (i.e., [3.0 M and 5.0 M], the active dissolution of Cu became completely dominant commencing at lower potentials as the [Cl^-] increased. The absence of oxides was confirmed by the current on the reverse scan which retraced that on the forward scan, showing no evidence of the reduction of surface films. This transition from passive oxide formation to $CuCl_x^{(x-1)-}$ dissolution required [Cl^-] >[BO_3]$_{tot}$.

Figure 7 compares the potentials, termed onset potentials, at which the current increased in a series of CVs similar to those shown in Figure 6. These potentials were obtained by recording the intersections between a horizontal line for zero current density and the tangent to the increasing current, as illustrated in Figure 6. Also included are

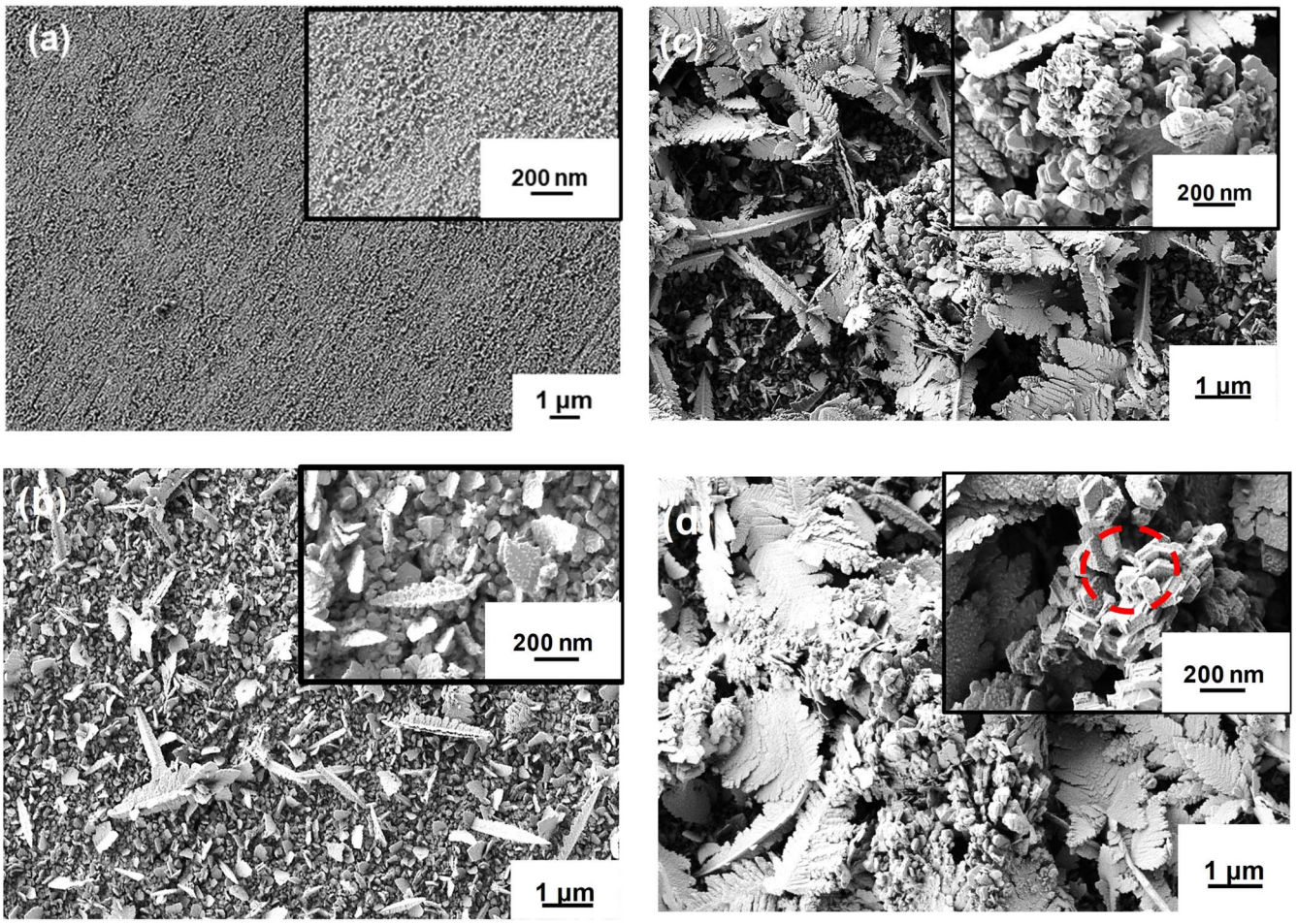

Figure 8. Morphologies of films on Cu after scanning E to different limits in solutions (pH 9) containing 0.1 M NaCl + 2×10^{-4} M Na_2S + 0.2 M borate: (a) −0.80 V vs SCE, (b) −0.40 V vs SCE, (c) −0.14 V vs SCE, (d) −0.10 V vs SCE.

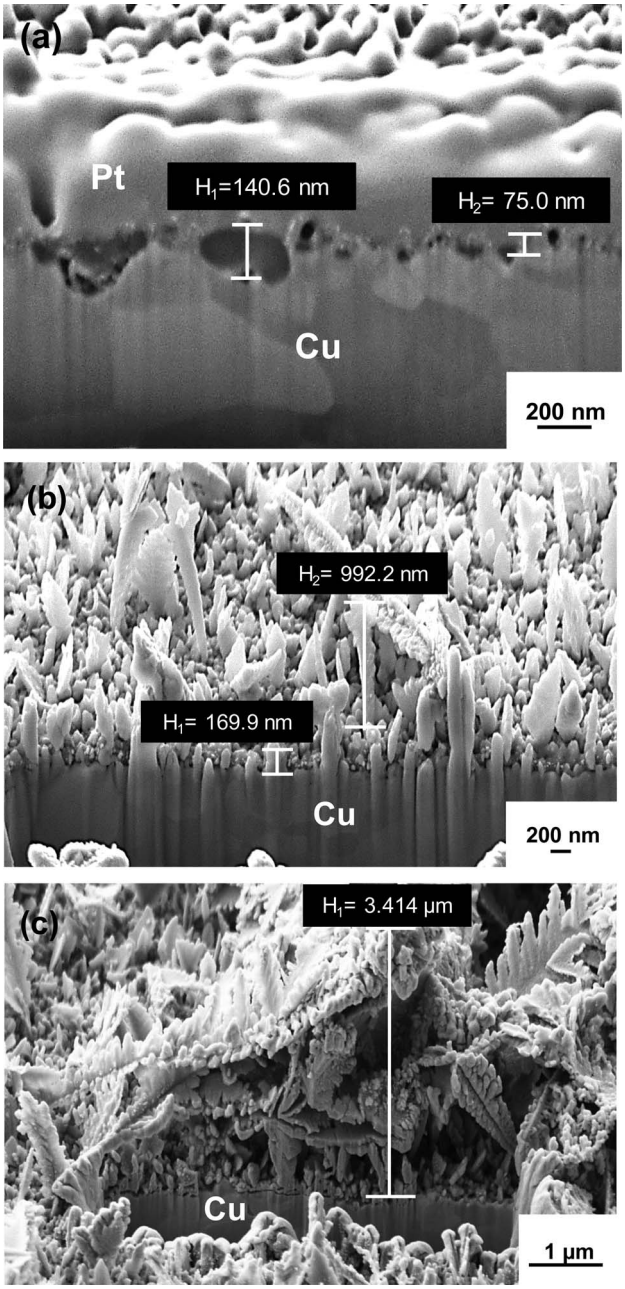

Figure 9. FIB cut cross-sections of films formed after scanning *E* to various limits in solutions containing 0.1 M NaCl, 2×10^{-4} M Na_2S, 0.2 M borate. (a) −0.80 V vs SCE, (b) −0.40 V vs SCE, and (c) −0.14 V vs SCE.

the potentials which Mao et al.[9] claimed are Cl^- induced breakdown potentials for the Cu_2S films grown at the lower potentials in region 1. The breakdown potentials claimed by Kong et al.[11] for experiments conducted in solutions containing a number of different anions (F^-, Cl^-, Br^-, I^-) also fell in this oxide-dominated potential region. The similarity between the two sets of values, for $[Cl^-] \geq 0.1$ M, demonstrated that the values measured by Mao et al. represent either oxide film breakdown potentials or potentials for the onset of active dissolution (as $Cu(Cl)_x^{(x-1)-}$), not Cu_2S breakdown potentials. The deviations in the two sets of data at higher $[Cl^-]$ could reflect the differences in potential scan rate and electrode rotation rate between the two set of experiments.

Morphology and composition of surface films.—Figures 8 and 9 show a series of SEM surface images and FIB-cut cross sections for films grown after scanning the potential to various limits at rotation rate $\omega = 33$ Hz. At $E = -0.80$ V vs SCE (in region 1, Figure 3) a very thin nodular film was formed. Since such a thin film was difficult to cross section, due to its immediate decomposition under both electron and Ga ions beams,[8] it was plated with Pt prior to attempting the FIB cut, which reduced the resolution of the image. The cross section, Figure 9a showed the Cu_2S film was approximately 75 to 150 nm thick, porous and deposited on a rough Cu interface.

When the film growth potential was increased to −0.4 V vs SCE, a scattered dendritic Cu_2S deposit, similar to that observed by Kong et al.[11] was formed on top of a porous, non-protective base layer, Figure 8b. Inspection of the FIB-cut cross section, Figure 9b, shows a coverage of the surface by a columnar film ranging in thickness from ∼ 170 nm to ∼ 990 nm. As demonstrated previously, Cu transport can occur in the form of either $Cu(SH)_2^-$ complexes or Cu_3S_3 particles,[29] a process that occurred so readily that any base layer present, but not visible on the scale of this image, was universally porous with pores on a scale of many nanometers or greater. The Cu surface exhibited a roughness on the scale of tens of nanometres with no visible localized pits.

Further increasing the applied potential to −0.14 V vs SCE led to a considerably thicker dendritic deposit confirming the on-going transport of Cu^I from the anodically oxidized Cu surface, Figure 8c. Examination of the FIB-cut cross sections after anodic oxidation at $E > -0.14$ V vs SCE, Figure 9c, shows that, as the Cu oxidation rate increased, previously grown Cu_2S layers appeared to be detached and replaced. This was to be expected since the Pilling-Bedworth ratio ($\Re_{PB}$) for Cu_2S growth on Cu is extremely large ($\Re_{PB} = 2$),[8] leading to large interfacial stresses as the applied potential was increased. The further deposition of dendritic structures within the void space created confirmed that the Cu surface remained an un-passivated source of $Cu(SH)_2^-$ and Cu_3S_3 formation. While no meaningful measurement of film thickness could be made, the dimensions of the deposits are indicated in Figure 9c.

When the applied *E* was in regions 2 and 3, the surface became covered by a thick dendritic deposit and a second deposit comprised of small hexagonal platelets, Figures 8c and 8d. To determine the composition of this deposit, an EDX analysis was performed on a cluster of such platelets (within the area marked with a red circle in Figure 8d). To minimize the analytical depth and obtain a more representative analysis, the acceleration voltage of the primary electrons was maintained at 5 kV. The EDX spectrum exhibited strong signals for both O and S confirming the presence of Cu_2S as well as Cu oxides. The percentages by weight of O and S were 1.38% and 12.46%, respectively. This platelet morphology could have indicated the initial formation of oxides followed by their subsequent partial conversion to Cu_2S, a process shown previously to occur.[31] The absence of Cl^- in this spectrum, and in others recorded on surfaces oxidized in regions 2 and 3, suggested that insignificant formation of CuCl occurred, consistent with the observation in Figure 1 that oxide formation dominated in regions 2 and 3 in a solution containing 0.2 M borate.

Representative examples of a series of Raman spectra collected at various surface locations are shown in Figure 10 for applied potentials in regions 1 (−0.4 V vs SCE) and 2 (−0.14 V vs SCE). As indicated on the figure, peaks at 147 cm^{-1}, 297 cm^{-1}, 525 cm^{-1} and 625 cm^{-1} were attributed to Cu_2O,[22,35–38] while peaks at ∼ 210 cm^{-1} and 300 cm^{-1} confirmed the presence of Cu_2S.[31,39–41] The peak at ∼297 cm^{-1} could also have indicated the presence of CuO since its formation was thermodynamically possible according to the *E*-pH diagram.[42] The very faint peaks in the range 800 cm^{-1} to 1400 cm^{-1} after scanning to −0.14 V vs SCE, have been observed before for anodically grown oxides on Cu[31] but remain unassigned. The very faint response in the region 525 cm^{-1} to 625 cm^{-1} after scanning to only −0.4 V vs SCE may indicate a small amount of Cu_2S decomposition to oxides induced by the laser beam during the recording of the Raman spectrum.

To confirm whether phases involving both oxidation states of Cu (Cu^I and Cu^{II}) were formed, followed by at least partial conversion to Cu_2S in regions 2 and 3, $Cu2p_{3/2}$ and Cu $L_3M_{4,5}M_{4,5}$ (Auger) XPS spectra were recorded on Cu samples prepared by scanning the

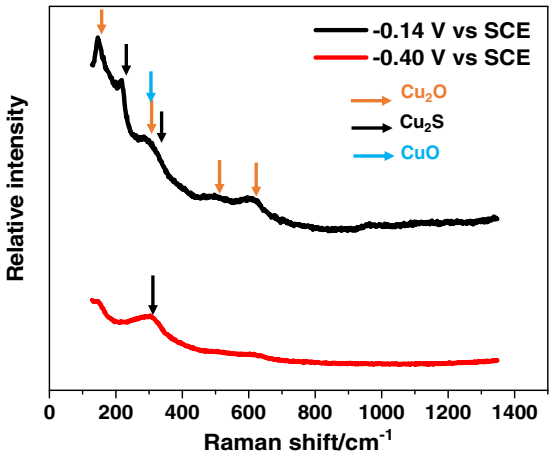

Figure 10. Raman spectra recorded on two Cu samples, indicating the presence of Cu_2O, CuO and Cu_2S.

potential to −0.14 V vs SCE and −0.1 V vs SCE in a solution containing 0.1 M NaCl, 0.2 M borate and 2×10^{-4} M SH^- at an electrode rotation rate of 33 Hz. The Cu^I/Cu^{II} ratio in the oxidized surface was calculated from the photoelectron yields for both the Cu $2p_{3/2}$ and satellite peaks, Figure 11 (A and B, respectively).[17] This calculation considers that the main emission line A contains contributions from both Cu oxidation states (Cu^I/Cu^{II}) but the intensity of the shake-up satellite peak contains a contribution from Cu^{II} only. To confirm these analyses, and to identify the various Cu species present, the Cu $L_3M_{4,5}M_{4,5}$ Auger spectrum was fitted as described elsewhere.[17] As indicated by the values on Figures 11b and 11d panels (in at%) the relative fractions (in the surface of the deposit) of Cu^I and Cu^{II} from Cu $L_3M_{4,5}M_{4,5}$ Auger spectra align well with the Cu $2p_{3/2}$ XPS analyses, Figures 11a and 11c. These results indicate that the small hexagonal platelets are oxides not sulfide, possibly undergoing a slow conversion. As expected, and in agreement with the Raman analysis, Cu_2O was the dominant phase present with significant amounts of Cu^{II}, as $Cu(OH)_2$, also present. While this cannot confirm passivity was due to Cu^{II} surface phases, it demonstrated their formation in this potential region did occur.

Reaction mechanism.—Figure 12 attempts to summarize the reactions which occurred in potential regions 1 to 3 (as defined in Figure 3). In region 1, while the formation of a thin passive layer may initially have been attempted (step a), as demonstrated previously,[8] the rapid development of interfacial stresses led to the immediate development of porosity. This enabled the release of anodically formed Cu(SH)(ads) species to solution as soluble complexes ($Cu(SH)_2^-$) and Cu_3S_3 clusters (step b). These species were then transported to the film solution interface and deposited as Cu_2S (step c). This process was partially controlled by the transport of SH^- to the Cu surface (step d) and by competition for surface adsorption sites with Cl^- (step e).

In region 2 (Figure 3), formation of CuCl species on the Cu surface (step f) led to the release of $CuCl_2^-$ to the solution within pores in the Cu_2S deposit (step g). In the buffered borate solution, Cu(OH)(ads) species also formed (step h), with the relative coverages dictated by

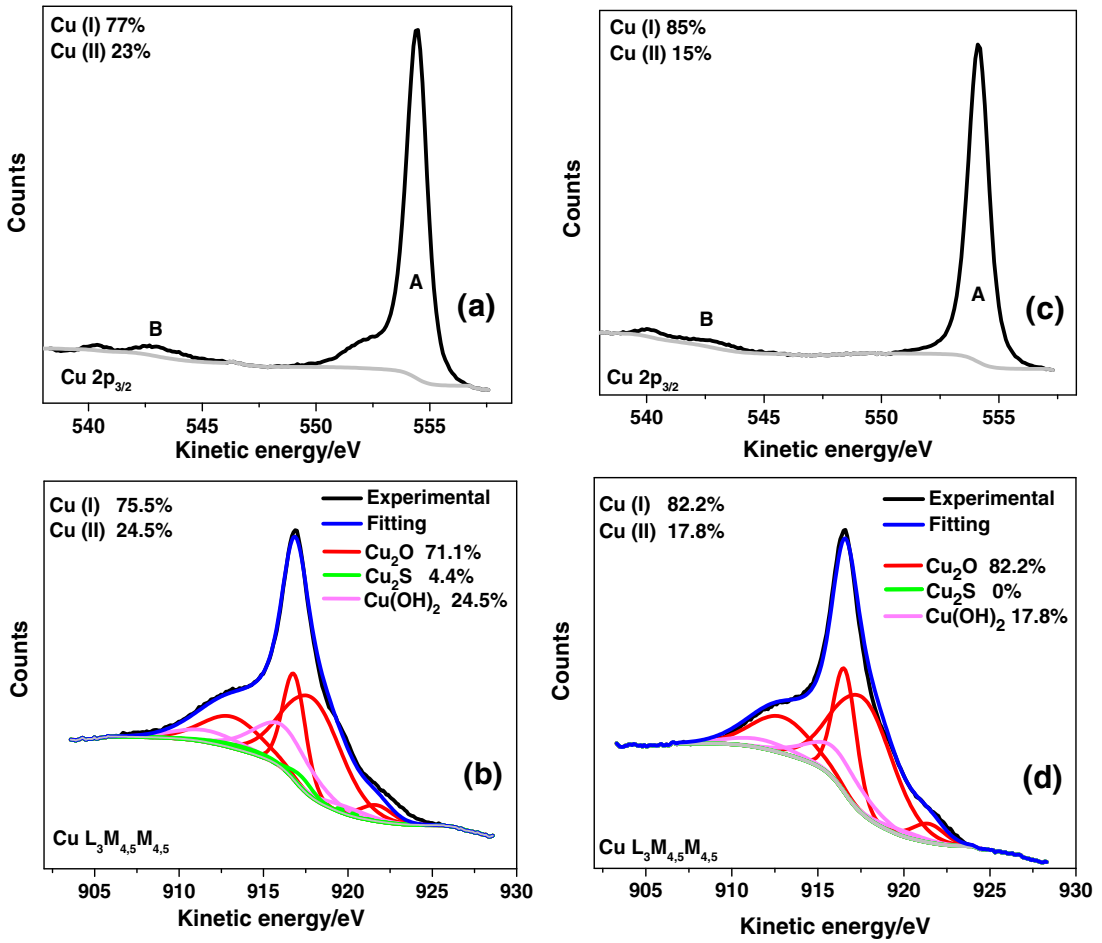

Figure 11. Cu $2p_{3/2}$ ((a) and (c)) and Cu $L_3M_{4,5}M_{4,5}$ ((b) and (d)) spectra from two Cu samples after potentiodynamically polarized to −0.14 V vs SCE ((a) and (b)) and −0.10 V vs SCE ((c) and (d)).

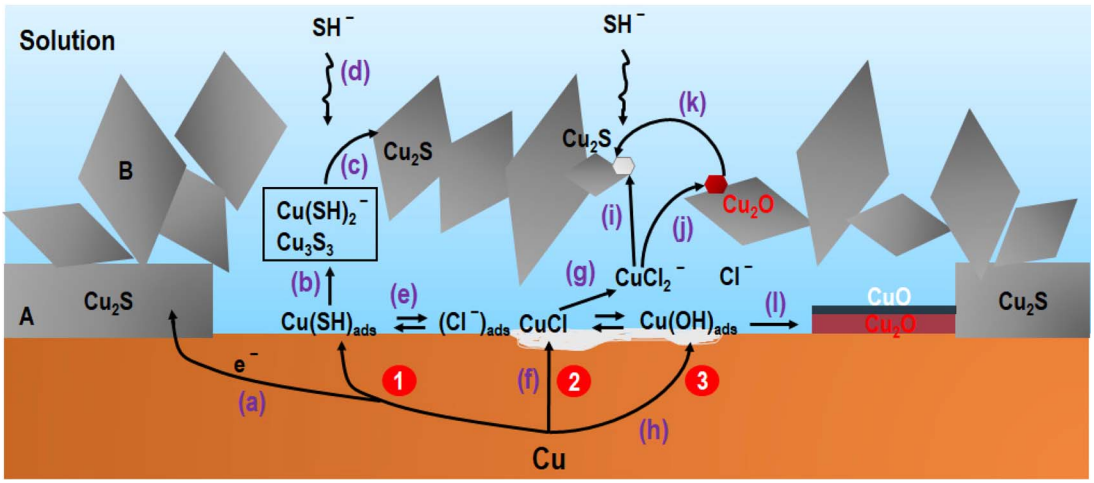

Figure 12. Schematic illustration of the film formation mechanism.: 1 – formation of a copper sulfide film in potential region 1 (Figure 3); 2 – the formation of copper chloride complexes in potential region 2 (Figure 3); 3 – formation of an oxide film in region 3 (Figure 3). Numbers 1 to 3 refer to the dominant reaction that is likely to occur at a specific regime of potentials. Each letter, as indicated from (a) to (g), represents each reaction and its associated chemical species.

the $[Cl^-]/[BO_3]_{tot}$ ratio. On transport to the film/solution interface, where SH^- was not depleted, the conversion of $CuCl_2^-(aq)$ to Cu_2S was likely (step i). Also, in the borate-buffered solution, Cu^I would have had limited solubility and could have deposited as Cu_2O (step j). Since Cu_2O would have been unstable in the presence of $SH^-(aq)$, its conversion to $Cu_2S(s)$ was expected (step k) but appeared to be slow.

In region 3, the direct formation of Cu_2O (step l), and possibly CuO, led to passivation provided the $[Cl^-]/[BO_3]_{tot}$ was sufficiently low.

Conclusions

As anticipated based on thermodynamic expectations, Cu_2S films were formed at potentials considerably lower than those at which anodic dissolution and oxide film formation occurred. The Cu_2S films were porous and non-passivating with the rate of film growth determined by a combination of SH^- transport through the growing film and the competition between SH^- and Cl^- for adsorption sites on the reacting Cu surface. No influence of borate on the Cu_2S film growth process was detected.

At more positive potentials, a combination of anodic dissolution as $CuCl_x^{(x-1)-}$ and oxide film formation (Cu_2O and possibly CuO) occurred, irrespective of whether a Cu_2S film had been grown at lower potentials. The balance between anodic dissolution and oxide film formation depended on the $[BO_3]_{tot}/[Cl^-]$ ratio with passivation by oxide film formation dominating when $[BO_3]_{tot} > [Cl^-]$. The measured onset potentials for anodic dissolution/oxide formation were close to the values measured by other authors and erroneously attributed to Cl^- induced breakdown of a passive Cu_2S film formed at lower potentials.

That the Cu_2S film remained porous and non-passive was confirmed by the revival of partially transport controlled Cu_2S growth once any oxide films formed at more positive potentials had been removed. No evidence for pitting was observed at any potential and would only be expected at potentials sufficiently positive for oxide formation.

Acknowledgments

This research was funded by Svensk Kärnbränslehantering AB (Solna, Sweden), Posiva Oy (Olkiluoto, Finland) and the Nuclear Waste Management Organization (Toronto, Canada). Authors thank Mary Jane Walzak (Surface Science Western) and Todd Simpson (Western Nanofabrication Facility) for performing Laser Raman Spectroscopy and SEM/FIB analyses, and for many useful discussions.

ORCID

M. Guo https://orcid.org/0000-0002-3731-1983
J. Chen https://orcid.org/0000-0003-4021-7127
T. Martino https://orcid.org/0000-0003-4710-968X
J. J. Noël https://orcid.org/0000-0003-3467-4778

References

1. Long-term safety for the final repository for spent nuclear fuel at Forsmark–Main report of the SR-Site project, *Svensk Kärnbränslehantering AB*, Technical Report TR 11-01, 2011.
2. F. King, D. S. Hall, and P. G. Keech, "Nature of the near-field environment in a deep geological repository and the implications for the corrosion behavior of the container," *Corros. Eng. Sci. Technol.*, **52**, 25 (2017).
3. F. King, C. Lilja, K. Pedersen, P. Pitkänen, and M. Vähänen, "An update of the state-of-the-art report on the corrosion of copper under expected conditions in a deep geologic repository," *Svensk Kärnbränslehantering AB*, Technical Report TR 10–67, 2010.
4. E.-L. Tullborg, J. Smellie, A.-C. Nilsson, M. J. Gimeno, L. Auqué, V. Brüchert, and J. Molinero, SR-Site – sulfide content in the groundwater at Forsmark, *Svensk Kärnbränslehantering AB*, Technical Report TR 10–39, 2010.
5. J. Chen, Z. Qin, T. Martino, and D. W. Shoesmith, "Effect of chloride on Cu corrosion in anaerobic sulfide solutions," *Corros. Eng. Sci. Technol.*, **52**, 40 (2017).
6. J. Chen, Z. Qin, and D. W. Shoesmith, "Key parameters determining structure and properties of sulfide films formed on copper corroding in anoxic sulfide solutions," *Corros. Eng. Sci. Technol.*, **49**, 415 (2014).
7. T. Martino, J. Chen, Z. Qin, and D. W. Shoesmith, "The kinetics of film growth and their influence on the susceptibility to pitting of copper in aqueous sulfide solutions," *Corros. Eng. Sci. Technol.*, **52**, 61 (2017).
8. T. Martino, R. Partovi-Nia, J. Chen, Z. Qin, and D. W. Shoesmith, "Mechanisms of film growth on copper in aqueous solutions containing sulfide and chloride under voltammetric conditions," *Electrochimica Acta.*, **127**, 439 (2014).
9. F. Mao, C. Dong, S. Sharifi-Asl, P. Lu, and D. D. Macdonald, "Passivity breakdown on copper: influence of chloride ion," *Electrochimica Acta.*, **144**, 391 (2014).
10. C. Dong, F. Mao, S. Gao, S. Sharifi-Asl, P. Lu, and D. D. Macdonald, "Passivity Breakdown on Copper: Influence of Temperature," *J. Electrochem. Soc.*, **163**, C707 (2016).
11. D. C. Kong, C. F. Dong, X. Q. Ni, A. N. Xu, C. He, K. Xiao, and X. G. Li, "Long-term polarisation and immersion for copper corrosion in high-level nuclear waste environment," *Mater. Corros.*, **68**, 1070 (2017).
12. D. Kong, C. Dong, X. Wei, C. Man, X. Lei, F. Mao, and X. Li, "Size matching effect between anion vacancies and halide ions in passive film breakdown on copper," *Electrochimica Acta.*, **292**, 817 (2018).
13. M. G. de Chialvo, R. C. Salvarezza, D. V. Moll, and A. J. Arvia, "Kinetics of passivation and pitting corrosion of polycrystalline copper in borate buffer solutions containing sodium chloride," *Electrochimica Acta.*, **30**, 1501 (1985).
14. U. Bertocci, "An EQMB examination of Cu surface oxides in borate buffer," *Electrochimica Acta.*, **49**, 1831 (2004).
15. W. Qafsaoui, G. Mankowski, and F. Dabosi, "The pitting corrosion of pure and low alloyed copper in chloride-containing borate buffered solutions," *Corros. Sci.*, **34**, 17 (1993).
16. Z. Qin, R. Daljeet, M. Ai, N. Farhangi, J. J. Noël, S. Ramamurthy, D. Shoesmith, F. King, and P. Keech, "The active/passive conditions for copper corrosion under nuclear waste repository environment," *Corros. Eng. Sci. Technol.*, **52**, 45 (2017).

17. M. C. Biesinger, "Advanced analysis of copper X-ray photoelectron spectra," *Surf. Interface Anal.*, **49**, 1325 (2017).
18. G. Kear, B. D. Barker, and F. C. Walsh, "Electrochemical corrosion of unalloyed copper in chloride media—-a critical review," *Corros. Sci.*, **46**, 109 (2004).
19. H. Y. H. Chan, C. G. Takoudis, and M. J. Weaver, "Oxide film formation and oxygen adsorption on copper in aqueous media as probed by surface-enhanced Raman spectroscopy," *J. Phys. Chem. B*, **103**, 357 (1999).
20. H. Y. H. Chan, C. G. Takoudis, and M. J. Weaver, "Electrochemical Control of Gas-Phase Oxidation and Reduction of Copper as Probed by Surface-Enhanced Raman Spectroscopy," *Electrochem. Solid-State Lett.*, **2**, 189 (1999).
21. R. L. Frost, "Raman spectroscopy of selected copper minerals of significance in corrosion," *Spectrochim. Acta. A. Mol. Biomol. Spectrosc.*, **59**, 1195 (2003).
22. J. C. Hamilton, J. C. Farmer, and R. J. Anderson, "In situ Raman spectroscopy of anodic films formed on copper and silver in sodium hydroxide solution," *J. Electrochem. Soc.*, **133**, 739 (1986).
23. H. Hagemann, H. Bill, E. Walker, and M. François, "Raman spectra of single crystal CuO," *Solid State Commun.*, **73**, 447 (1990).
24. I. Puigdomenech and C. Taxén, "Thermodynamic data for copper. Implications for the corrosion of copper under repository conditions," *Svensk Kärnbränslehantering AB*, Technical Report TR 00–13, 2000.
25. C. F. Baes and R. E. Mesmer, The Hydrolysis of Cations Wiley, N. Y. 177 (1976).
26. D. A. Palmer, "Solubility measurements of crystalline Cu2O in aqueous solution as a function of temperature and pH," *J. Solut. Chem.*, **40**, 1067 (2011).
27. J. Smith, Z. Qin, F. King, L. Werme, and D. W. Shoesmith, "Sulfide film formation on copper under electrochemical and natural corrosion conditions," *Corrosion.*, **63**, 135 (2007).
28. T. Martino, J. Smith, J. Chen, Z. Qin, J. J. Noël, and D. W. Shoesmith, "The Properties of Electrochemically-Grown Copper Sulfide Films," *J. Electrochem. Soc.*, **166**, C9 (2019).
29. J. Chen, Z. Qin, T. Martino, M. Guo, and D. W. Shoesmith, "Copper transport and sulfide sequestration during copper corrosion in anaerobic aqueous sulfide solutions," *Corros. Sci.*, **131**, 245 (2018).
30. G. W. Luther, S. M. Theberge, T. F. Rozan, D. Rickard, C. C. Rowlands, and A. Oldroyd, "Aqueous copper sulfide clusters as intermediates during copper sulfide formation," *Environ. Sci. Technol.*, **36**, 394 (2002).
31. J. M. Smith, J. C. Wren, M. Odziemkowski, and D. W. Shoesmith, "The electrochemical response of preoxidized copper in aqueous sulfide solutions," *J. Electrochem. Soc.*, **154**, C431 (2007).
32. D. Kong, C. Dong, M. Zhao, X. Ni, C. Man, and X. Li, "Effect of chloride concentration on passive film properties on copper," *Corros. Eng. Sci. Technol.*, **53**, 122 (2018).
33. P. Broekmann, M. Wilms, M. Kruft, C. Stuhlmann, and K. Wandelt, "In-situ STM investigation of specific anion adsorption on Cu (111)," *J. Electroanal. Chem.*, **467**, 307 (1999).
34. L.-J. Wan and K. Itaya, "In situ scanning tunneling microscopy of Cu (110): atomic structures of halide adlayers and anodic dissolution," *J. Electroanal. Chem.*, **473**, 10 (1999).
35. P. Ropret and T. Kosec, "Raman investigation of artificial patinas on recent bronze–Part I: climatic chamber exposure," *J. Raman Spectrosc.*, **43**, 1578 (2012).
36. T. Kosec, Z. Qin, J. Chen, A. Legat, and D. W. Shoesmith, "Copper corrosion in bentonite/saline groundwater solution: Effects of solution and bentonite chemistry," *Corros. Sci.*, **90**, 248 (2015).
37. A. Björkbacka, C. M. Johnson, C. Leygraf, and M. Jonsson, "Role of the Oxide Layer in Radiation-Induced Corrosion of Copper in Anoxic Water," *J. Phys. Chem. C*, **120**, 11450 (2016).
38. J. Turnbull, R. Szukalo, M. Behazin, D. Hall, D. Zagidulin, S. Ramamurthy, J. C. Wren, and D. W. Shoesmith, "The Effects of Cathodic Reagent Concentration and Small Solution Volumes on the Corrosion of Copper in Dilute Nitric Acid Solutions," *Corrosion*, **74**, 326 (2017).
39. A. Kudelski, "Structures of monolayers formed from different HS—(CH2) 2—X thiols on gold, silver and copper: comparitive studies by surface-enhanced Raman scattering," *J. Raman Spectrosc.*, **34**, 853 (2003).
40. G. Parker, G. A. Hope, and R. Woods, "Raman spectroscopic identification of surface species in the leaching of chalcopyrite," *Colloids Surf A*, **318**, 160 (2008).
41. R. Woods, G. A. Hope, and K. Watling, "A SERS spectroelectrochemical investigation of the interaction of 2-mercaptobenzothiazole with copper, silver and gold surfaces," *J. Appl. Electrochem.*, **30**, 1209 (2000).
42. F. King, L. Ahonen, C. Taxén, U. Vuorinen, and L. Werme, "Copper corrosion under expected conditions in a deep geologic repository," *Svensk Kärnbränslehantering AB*, Technical Report TR 01–23, 2001.